BNL-112128-2016-CP

# *Second Generation Coil Design of the $Nb_3Sn$ Low-β Quadrupole for the High Luminosity LHC*

**S. Izquierdo Bermudez, G. Ambrosio, A. Ballarino, E. Cavanna, R. Bossert, D. Cheng, D. Dietderich, P. Ferracin, A. Ghosh, P. Hagen, E. Holik, J. C. Perez, E. Rochepault, J. Schmalzle, E. Todesco and M. Yu**

*Presented at the 24th International Conference on Magnet Technology (MT24)*
Seoul, Korea
October 18-23, 2015

*Accepted for Publication in IEEE Transactions on Applied Superconductivity, January 2016*

April 2016

**The Superconducting Magnet Division**

**Brookhaven National Laboratory**

**U.S. Department of Energy**
**Office of Science, High Energy Physics**

# DISCLAIMER

# Second Generation Coil Design of the $Nb_3Sn$ low-$\beta$ Quadrupole for the High Luminosity LHC

S. Izquierdo Bermudez, G. Ambrosio, A. Ballarino, E. Cavanna, R. Bossert, D. Cheng, D. Dietderich, P. Ferracin, A. Ghosh, P. Hagen, E. Holik, J. C. Perez, E. Rochepault, J. Schmalzle, E. Todesco and M. Yu

***Abstract*—As part of the Large Hadron Collider Luminosity upgrade (HiLumi-LHC) program, the US LARP collaboration and CERN are working together to design and build a 150 mm aperture $Nb_3Sn$ quadrupole for the LHC interaction regions. A first series of 1.5 m long coils were fabricated and assembled in a first short model. A detailed visual inspection of the coils was carried out to investigate cable dimensional changes during heat treatment and the position of the windings in the coil straight section and in the end region. The analyses allow identifying a set of design changes which, combined with a fine tune of the cable geometry and a field quality optimization, were implemented in a new, second-generation, coil design. In this paper we review the main characteristics of the first generation coils, describe the modification in coil lay-out, and discuss their impact on parts design and magnet analysis.**

***Index Terms*—LHC upgrade, $Nb_3Sn$ Magnet, Superconducting Accelerator Magnets, Coil End Design.**

## I. Introduction

THE high luminosity LHC upgrade aims at increasing the integrated luminosity of the LHC by a factor of 10 beyond its nominal performance expected for 2023 [1]. Part of the upgrade relies on the replacement of the single aperture quadrupoles in the interaction region (the so called low-$\beta$ or inner triplet quadrupoles). The design, referred as MQXF, considers a 150 mm aperture quadrupole based on $Nb_3Sn$ technology [2]. MQXF is currently being developed in a joint collaboration between CERN and the US-LHC Accelerator Research Program (LARP), and it benefits from the 10 years of development of $Nb_3Sn$ technology by LARP [3].

Since Summer 2013, when the geometry of the first iteration cable was fixed, a total of 13 coils were fabricated. Coil production is summarized in Table I. Following a cable R&D program, the cable geometry was changed in order to limit the current degradation during cabling. This second iteration of cable geometry provided also the opportunity to implement a set of additional design improvements such as the introduction of the capability to fine tune the field quality after construction of the first models through coil shimming and the magnetic re-optimization of the coil ends to account for the contribution of the $Nb_3Sn$/Nb-Ti splice and leads. Here, we review the main characteristics of the first generation coils and describe the changes implemented in the MQXFS second generation coil series.

TABLE I
SUMMARY OF MQXFS COIL PRODUCTION FOR THE FIRST GENERATION DESIGN

| Coil | Strand | Producer | Status/Comment |
|---|---|---|---|
| 1 | RRP108/127 | LARP | Practice coil, destructive inspection |
| 2 | RRP108/127 | LARP | Coil tested in mirror structure |
| 3 | RRP108/127 | LARP | Coil assembled in the first model |
| 4 | RRP108/127 | LARP | Swapped spacers, impregnation test |
| 5 | RRP108/127 | LARP | Coil assembled in the first model |
| 6 | RRP108/127 | LARP | Reserve coil |
| 000 | Copper | CERN | Practice coil |
| 101 | RRP132/169 | CERN | Practice coil, destructive inspection |
| 102 | RRP132/169 | CERN | Reserve coil, weak splice |
| 103 | RRP132/169 | CERN | Coil assembled in the first model |
| 104 | RRP132/169 | CERN | Coil assembled in the first model |
| 201 | PIT192 | CERN | Practice coil |
| 201 | PIT192 | CERN | Practice coil |

## II. Review Of The First Generation Coils

MQXF coils are made with a Rutherford-type cable composed of 40 $Nb_3Sn$ strands of 0.85 mm diameter. The cable incorporates a 12 mm wide stainless steel core of 25 $\mu$m thickness to reduce inter-strand coupling currents. Powder-in-tube (PIT) strands by Bruker-EAS and Restacked-Rod Process (RRP) by Oxford Superconducting Technology (OST) are used. The cable is insulated with braided S2 glass, with a target thickness at 5 MPa of 0.150 mm. Insulation thickness is systematically measured for each coil using 10 cables stacks. The measured insulation thickness is 146 $\pm$ 3 $\mu$m for CERN coils and 143 $\pm$ 3 $\mu$m for LARP coils.

The coil fabrication is based on the technology developed in HQ, the LARP quadrupole with a 120 mm bore [4]. The manufacturing process is composed of four main steps: 1) winding with an unreacted cable; 2) application and curing at 150°C of a ceramic binder CTD-1202X to make the coil easy to handle; 3) heat treatment at about 650°C to form $Nb_3Sn$, 4) vacuum impregnation with Epoxy resin CTD-101K to provide mechanical stability to the coil. Before impregnation, a flexible

Manuscript submitted 10th Oct 2015. Research supported by EU FP7 HiLumi LHC - Grant Agreement 284404

S. Izquierdo Bermudez, A. Ballarino, P. Hagen, P. Ferracin, J. C. Perez, E.Rochepault and E.Todesco are with CERN, 1211 Geneva, Switzerland (e-mail: susana.izquierdo.bermudez@cern.ch).

E. Cavanna is with ASG Superconductors S.p.A.

G. Ambrosio, R. Bossert, E. Holik and M. Yu are with Fermi National Accelerator Laboratory (FNAL), Batavia, IL 60510 USA.

D. Cheng and D. Dietderich are with Lawrence Berkeley National Laboratory (LBNL), Berkley, CA 94720 USA.

J. Schmalzle and A. Ghosh are with Brookhaven National Laboratory (BNL), Upton, NY 11973 USA.

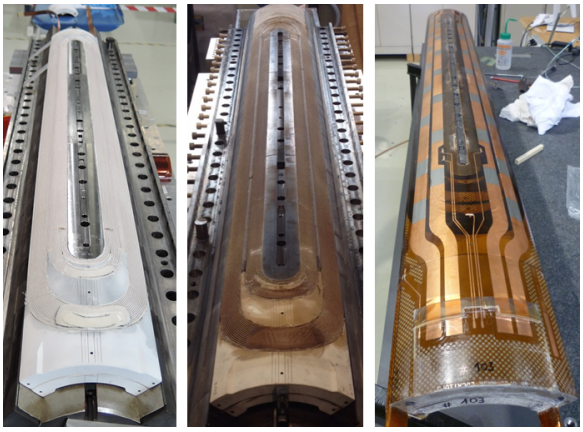

Fig. 1. Coil at different stages of the manufacturing process. From left to right: after curing (2), after reaction (3) and after impregnation (4).

circuit which includes quench protection heaters and voltage taps is placed on the coil inner and outer radius. Nb-Ti leads are also soldered to the $Nb_3Sn$ cable before impregnation, using $Sn_{96}Ag_4$ solder and a non-halide activated flux. Figure 1 shows a coil at different steps of the manufacturing process.

The formation of the superconducting phase $Nb_3Sn$ produces a volume expansion leading to radial, azimuthal and axial dimensional changes of the conductor due to heat treatment. In order to avoid coil over-compaction, and based on HQ experience [5], the cavity of the curing, reaction and impregnation tooling is designed accounting for 4.5% cable expansion in thickness and 2% in width. In order to allow the coil to contract longitudinally, the pole piece around which the coil is wound is made of three parts separated by a gap. Gap contraction due to winding tension relaxation is in between 1.2-1.6 mm for CERN and LARP coils. Pole gap contraction during reaction is less than 0.5 mm for CERN coils and around 1.7 mm for LARP coils.

## III. Cable Parameters for Second Generation Design

The cable research and development process continued after the definition of the first generation cable design aiming at quantifying the performance of cables. The program was focused on maximizing the cable mechanical stability and minimizing the critical current and local RRR cabling degradation. As a result, an excessive critical current degradation due to cabling (from 6% to 8.6%) was found for the PIT cables, leading to a change on the cable geometry. The second generation cable has a keystone angle reduced from 0.55° to 0.40°, increasing the thickness of the thin edge by 24 $\mu$m, in order to bring the critical current degradation due to cabling to <5% for the PIT conductor and <3% for the RRP conductor. The same geometry of cable has been adopted for the RRP cables to enable a consistent magnet design.

A series of measurements were performed at CERN and LARP to characterize the conductor dimensional change during heat treatment. The investigation was performed on RRP 108/127, RRP 132/169 and PIT 192 conductors using different set ups, from the strand level to the actual coil cross section [6]. The radius of un-confined bare strands was first measured before and after heat treatment. The average radius expansion is 1.8% for the RRP wires and 1.6% for the PIT.

Non-insulated single cables have also been measured. The cables are left free to expand or contract in all directions, but they are held in position during reaction to prevent any unwrapping. The width expansions (respectively 1.7% and 1.5% for RRP and PIT) are consistent with radius expansions of single strands. The thickness increase is larger (respectively 2.5% and 3.0%). However, in both cases, the conductor cross section expansion is similar (respectively 4.2% and 4.5%). The values are in good agreement with other measurements done on MQXF un-confined 10-stacks [7].

These tests were compared with stacks of insulated cables. The cables are in this case insulated and locked transversally into position by the tooling. The cavity is 4.5% larger in thickness and 2% larger in width to reproduce the actual configuration of the conductors in the coil during reaction. The measured thickness expansion is 2.5%, determined by measuring the difference on thickness of a stack of ten conductors before and after reaction. An accurate measurement of the cable width was not possible using this set up.

Measurements of coil cross sections were finally taken from the first practice LARP and CERN coils. Different analysis methods show very consistent results for the two coils, with a thickness expansion of about 3.0% and only 0.15% expansion in width. As a consequence, conductors are aligned on the outer diameter and the $\approx 600$ $\mu$m of free radial space due to the overestimation in cable width expansion are filled with epoxy in a non-uniform way, which will have a negative impact on field quality. The large difference in width expansion in between the measurements on coil cross sections and non-insulated conductors was also observed in [7], where the dimensional change on the conductor was studied for different insulation schemes. Width expansion on cables with braided glass fibre insulation is less than 0.5%, conductors insulated with a sleeve expand about 1%. In MQXF the cable is insulated with braided S2 glass.

Based on this analysis, and in order to find the best compromise between performance and field quality, it was decided to: 1) reduce the radial space in the tooling to accommodate for a cable width expansion of 1.2% instead of 2%; 2) keep the same azimuthal space, corresponding to a thickness expansion of 4.5%. The reduction of the nominal insulation thickness by 5 $\mu$m without changing the insulation technique will help to assure a better azimuthal position of the coil turns. Table II compares the cable parameters for the first and second generation coil design.

## IV. Second Generation Coil Design

### A. Coil Design Constrains

MQXF is basically a scale-up in radius of HQ [8]. Coil cross section was optimized for stress distribution among layers and field quality [9]. In order to minimize the impact on coil fabrication and tooling, the guidelines for coil re-optimization were: 1) to keep same number of conductors per block; 2) to keep the pole turns of the inner and outer layer aligned so as to

TABLE II
CABLE PARAMETERS

| Parameters | $1^{st}$ Gen. | $2^{nd}$ Gen. | |
|---|---|---|---|
| Un-reacted bare cable width | 18.150 | 18.150 | mm |
| Un-reacted bare cable mid-thickness | 1.525 | 1.525 | mm |
| Reacted bare cable width | 18.513 | 18.363 | mm |
| Reacted bare cable mid-thickness | 1.594 | 1.594 | mm |
| Cable keystone angle | 0.550 | 0.400 | ◦ |
| Cable insulation thickness | 0.150 | 0.145 | mm |

have the same concept of layer jump (only hard way bending); 3) to keep the same coil inner and outer diameters. The free radial space due to the decrease on cable width after reaction will be partially absorbed by the inter-layer insulation (which increases from 0.500 mm to 0.660 mm) and the outer layer of S2-glass that is installed in the outer coil diameter before impregnation (which increases from 0.150 mm to 0.310 mm). For the second generation design, we also consider a thicker mid-plane and pole insulation to allow fine tuning of field quality. The insulation between the mid-plane and the first insulated conductor increases from 0.250 mm to 0.375 mm, and from 0.350 mm to 0.500 mm between the pole and the insulated conductor.

### B. 2D Magnetic Design

Due to the large beam size and orbit displacement in the final focusing triplet, these magnets have challenging targets for field quality requirements at nominal operating current. The coil cross section is optimized such that all allowed harmonics are within one unit at 6.5 TeV. Field quality is optimized at 123 T/m (6.5 TeV) because the triplet will operate between 100% and 90% of the maximum gradient (132.6 T/m, 7 TeV) [10]. The normal ($b_n$) and skew ($a_n$) components of the field harmonics are defined as,

$$\begin{aligned} B_y + iB_x = & \ \Sigma(B_n + iA_n)(x+iy)^{n-1} \\ & = 10^{-4} B_2 \ \Sigma(b_n + ia_n)\left(\frac{x+iy}{R_{ref}}\right)^{n-1} \end{aligned} \quad (1)$$

where $B_x$ and $B_y$ are the components of the field, $B_2$ the main field and $R_{ref}$ the reference radius, which is 2/3 of the aperture radius ($R_{ref}$= 50 mm). For the second generation design, coil cross section has been re-optimized to account for the effect of coil deformation on field quality [11] and the contribution of the splice and connection leads [12]. The impact of coil deformation is an offset of +0.9 units on $b_6$, mostly caused by the azimuthal coil deformation during cool down. The deformation due to electromagnetic forces have a negligible effect on $b_6$.

The nominal gradient has been decreased from 140 T/m to 132.6 T/m to increase the margin, decreasing the peak field on the coil from 12.1 T to 11.4 T. Table III summarizes the main coil and magnet parameters and Fig. 2 compares the conductor position of the first and second coil generation design.

TABLE III
MAGNET PARAMETERS FOR THE SECOND GENERATION DESIGN

| Parameters | | Units |
|---|---|---|
| Operational temperature | 1.9 | K |
| Clear aperture diameter | 150 | mm |
| Nominal gradient | 132.6 | T/m |
| Nominal current | 16.47 | kA |
| Nominal peak field on the coil | 11.4 | T |
| % load line at nominal gradient | 77 | % |
| $F_x/F_y$ (per octant) at nominal current | 2.47/-3.48 | MN/m |
| Stored energy at $I_{nom}$ | 1.17 | MJ/m |
| Differential inductance at $I_{nom}$ | 8.21 | mH/m |
| $b_6/b_{10}/b_{14}$ at $R_{ref}$ = 50 mm | -0.64/-0.11/-0.87 | units |

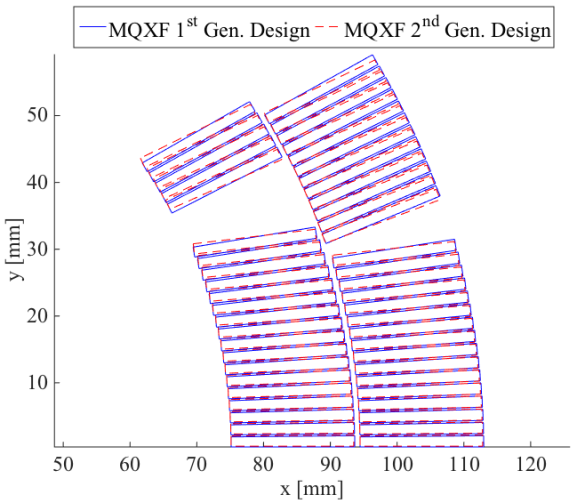


Fig. 2. Coil cross section. Comparison of the first and second generation coil design.

### C. Field Quality Correction Actions

The main concerns in terms of field quality are: 1) a systematic deviation on the first allowed harmonic, $b_6$, as the target range is only 1 unit; 2) the control of the low order, not allowed multipole (mainly $b_3$, $a_3$, $b_4$, $a_4$) stemming from assembly or component asymmetries. The plan is to correct the first allowed harmonic through shims at the level of the coil; the non-allowed harmonics will be corrected through ferromagnetic shims allocated in the yoke. The correcting capabilities of both techniques are discussed in this section.

*1) Coil shimming:* The fine tuning of the pole and mid-plane shim thickness to optimize the systematic components of field quality is a technique that was successfully applied during LHC production to control field quality [13]. The first section of Table IV shows the impact on $b_6$ and $b_{10}$ of the introduction of a 125 $\mu$m thickness shim placed in the pole or in the mid-plane during coil fabrication. Higher order multipoles are not affected. In order to modify the coil geometry without an impact of its state of compression (pre-stress), the preferred solution is to combine the introduction of a shim in the mid-plane with the reduction of the pole insulation thickness. Using this approach, the azimuthal coil position can be optimized without an impact on the coil compaction during reaction. The

TABLE IV
EFFECT OF A 125 $\mu$M SHIM ON THE ALLOWED MULTIPOLES ($10^{-4}$ UNITS, $R_{ref}$=50 MM)

| Coil shimming | Inner Layer | | Outer layer | |
|---|---|---|---|---|
| | $\Delta b_6$ | $\Delta b_{10}$ | $\Delta b_6$ | $\Delta b_{10}$ |
| Mid Plane (+) Pole (=) | -2.5 | -0.5 | -0.6 | 0.0 |
| Mid Plane (=) Pole (+) | +1.5 | -0.1 | +0.6 | 0.0 |
| Coil shimming | Inner Layer | | Outer layer | |
| | $\Delta b_6$ | $\Delta b_{10}$ | $\Delta b_6$ | $\Delta b_{10}$ |
| Mid Plane (+) Pole (-) | -4.3 | -0.5 | -1.3 | 0.0 |
| Mid Plane (-) Pole (+) | +3.9 | +0.5 | +1.4 | 0.0 |

second section of Table IV shows the impact on field quality of a coil rotation in the clockwise and anti-clockwise direction using a 125 $\mu$m shim. The nominal insulation thickness on the mid-plane and on the pole has been increased with respect to the first generation design to assure good electrical integrity for all the possible combinations.

*2) Ferro-magnetic shimming:* The correction of low order not allowed multipoles using magnetic shims is a technique that has been extensively been studied and tested in the past [14], [15]. The idea is to excite different configurations of field harmonics through an asymmetric placing of magnetic shims to compensate the coil geometric imperfections. A very careful assessment of the correlations between measurements at 300 K and in operational conditions is needed to carry out effective corrective actions.

Figure 3 shows the three different locations for magnetic shims that have been studied for MQXF. Electromagnetic computations show that shims on the collar rods have a strong impact at low current but they quickly saturate and get transparent at high field values [16]. Shims on the yoke alignment slot are too far from the beam so their correction capability is small. Ferromagnetic shims placed on the bladder slots can correct up to $\pm$5 units of $b_3$ and $a_3$, $\pm$3 units of $b_4$ and $\pm$1 units of $a_4$. Table V shows the set of correction schemes which can be used to correct individual sextupole and octupole field errors. In between brackets, the associated impact on the decapole is also shown. Higher order harmonics are not affected.

### D. 3D Magnetic Design

Magnetic and mechanical optimization of the coil ends for the first generation coil design is described in [12]. In order to minimize the impact on beam dynamics of the reduction of the nominal gradient from 140 T/m to 132.6 T/m, the magnetic length has been increased by 200 mm for Q1/Q3 and by 350 mm for Q2a/b. Table VI summarizes the most relevant magnetic and physical lengths for the short model and full size magnets.

Destructive inspection of the the first LARP and CERN coils was performed in order to quantify the quality of the winding. Figure 4 compares the actual position of the conductors on the return end of coil 101 with the theoretical location. The fitting is very good. Following the positive feedback from winding and destructive inspection, the overall shape of the coil ends

TABLE V
SHIM COMBINATIONS FOR THE CORRECTION OF THE SEXTUPOLE AND OCTUPOLE FIELD ERRORS ($10^{-4}$ UNITS, $R_{ref}$=50 MM)

| Shim combination | Multipole | Units |
|---|---|---|
| Bladder slots 1,2,3,8 | +$b_3$ [+$b_5$] | +3.2 [+0.2] |
| Bladder slots 4,5,6,7 | -$b_3$ [-$b_5$] | -3.2 [-0.2] |
| Bladder slots 1,2,4,7 | +$b_3$ [+$b_5$] | +5.2 [+0.6] |
| Bladder slots 3,5,6,8 | -$b_3$ [-$b_5$] | -5.2 [+0.6] |
| Bladder slots 1,2,5,6 | +$b_4$ | +2.8 |
| Bladder slots 3,4,7,8 | -$b_4$ | -2.8 |
| Bladder slots 1,3,4,6 | +$a_3$ [-$a_5$] | +5.2 [-0.6] |
| Bladder slots 2,5,7,8 | -$a_3$ [+$a_5$] | +5.2 [-0.6] |
| Bladder slots 1,4,5,8 | -$a_4$ | -0.8 |
| Bladder slots 2,3,6,7 | +$a_4$ | +0.8 |
| Bladder slots 1,6,7,8 | -$a_3$ [+$a_5$] | -3.1 [+0.2] |
| Bladder slots 2,3,4,5 | +$a_3$ [-$a_5$] | -3.1 [+0.2] |

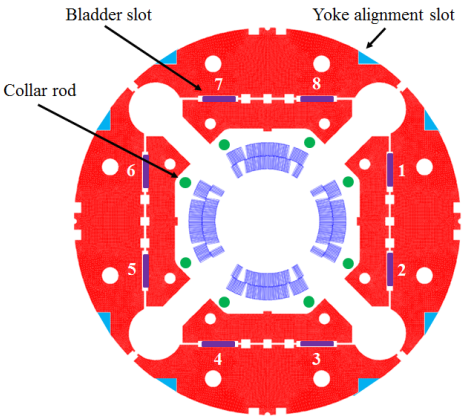


Fig. 3. Location of the ferromagnetic shims on the magnet cross section

was not modified. Only a fine tuning was needed to adapt to the new cable geometry and optimize field quality.

In order to compensate the non-negligible positive contribution of the coil layer jump and $Nb_3Sn$/Nb-Ti splice to $b_6$ [12], the following actions were taken: 1) the magnet longitudinal loading system has been moved from the connection side to the non-connection side of the magnet to minimize the length of the current leads [17]; 2) re-optimization of the longitudinal position of the coil blocks at the ends (Fig. 5 compares the conductor longitudinal position for the first and second generation design); 3) coil cross section has been optimized aiming to a $b_6$ close to -0.5 units in the straight section to minimize the $b_6$ integrated over the entire magnet length. Integrated field harmonics are computed following the convention,

$$\overline{b_n} = \frac{\int_{z_0}^{z_{end}} B_n(I,z)dz}{B_2^{ss} l_{mag}(I)} \tag{2}$$

where $B_n$ are computed as defined in Eq. 1, ${B_2}^{ss}$ is the main field in the straight section and $l_{mag}$ is the magnetic length of the integrated section,

$$l_{mag}(I) = \frac{1}{B_2^{ss}(I)} \int_{z_0}^{z_{end}} B_2(I,z)dz \tag{3}$$

TABLE VI
MAGNETIC AND PHYSICAL LENGTHS

| Parameters | Units | SQXFS | Q1/Q3 | Q2a/b |
|---|---|---|---|---|
| Magnetic length at 1.9 K | mm | 1196 | 4200 | 7150 |
| Cable unit length | m | 150 | 470 | 750 |
| Overall coil length at RT (including splice extension) | mm | 1510 | 4523 | 7481 |
| Magnetic yoke extension at RT | mm | 1550 | 4563 | 7521 |

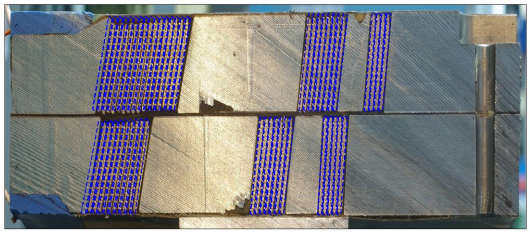

Fig. 4. Conductor position on coil ends for CERN coil 101.

Integration limits are $\pm\infty$ when providing the total integral of the harmonic content. The contribution of each magnet end is also provided in a separate column in Table VII. As it can be observed, even if the integral of $b_6$ over the connection side of 400 mm length is close to 9 units, the total integral is 0.32 units for Q1/Q3 and -0.07 units for Q2a/b. The rest of the harmonics are also summarized in the table, providing the local contribution on the magnet connection side (c.s.), non connection side (n.c.s.) and the total integral.

## V. CONCLUSIONS

A total of 13 MQXFS short coils have been produced using the first generation design. In this paper we describe the changes implemented in the second generation MQXFS coil series, which include: 1) a new cable geometry with a keystone angle reduced from 0.55° to 0.40° to minimize the critical current and the local RRR degradation due to cabling; 2) reduced operational gradient and longer magnetic length to increase the margin; 3) reduced conductor width expansion during heat treatment (from 2% to 1.2%); 4) thicker mid-plane and pole insulation thickness to allow fine tuning of field quality through coil shimming; 5) re-optimized block longitudinal position on the coil ends and reduction of the current leads length to minimize the integrated field harmonics; 6) re-optimized coil cross section which accounts for the impact of coil deformation on field quality (+0.9 units of $b_6$) and the 3D effects (+0.5 units of $b_6$).

TABLE VII
FIELD HARMONICS

| | Straight part | Ends | | Integral | |
|---|---|---|---|---|---|
| | | c.s | n.c.s | Q1/Q3 | Q2a/b |
| Mag. length (m) | – | 0.40 | 0.34 | 4.20 | 7.15 |
| $b_6$ | -0.64 | 8.94 | -0.03 | 0.32 | -0.07 |
| $b_{10}$ | -0.11 | -0.19 | -0.82 | -0.18 | -0.15 |
| $b_{14}$ | -0.87 | -0.55 | -1.08 | -0.86 | -0.86 |
| $a_2$ | 0.00 | -31.34 | 0.00 | -2.98 | -1.75 |
| $a_6$ | 0.00 | 2.21 | 0.00 | 0.21 | 0.12 |

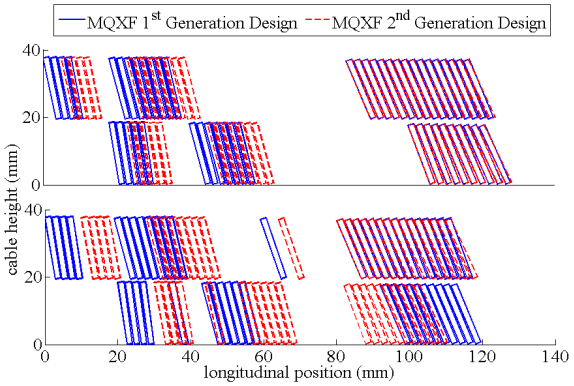


Fig. 5. Comparison of the conductor position on coil ends for the first and second generation coil design.

## REFERENCES


[1] "HL-LHC Preliminary Design Report," CERN-ACC-2014-0300, 28 November 2014.

[2] E. Todesco, et al., "Design studies for the low-beta quadrupoles for the LHC luminosity upgrade," *IEEE Trans. App. Supercond*, vol 23, no. 3, p. 4003305, June 2013.

[3] S. A. Gourlay, et al., "Magnet R&D for the US LHC accelerator research program," *IEEE Trans. Appl. Supercond.*, vol. 16, no. 2, pp. 324327, Jun. 2006.

[4] F. Borgnolutti et al., "Fabrication of a second-generation of $Nb_3Sn$ coils for the LARP HQ02 quadrupole magnet," *IEEE Trans. Appl. Supercond.*, vol. 24, no. 3, Jun. 2014, Art. ID. 4003005.

[5] H. Felice, et al., "Impact of coil compaction on $Nb_3Sn$ LARP HQ magnet," *IEEE Trans. Appl. Supercond.*, vol. 22, no. 3, Jun. 2012, Art. ID. 4001904.

[6] E. Rochepault, et al., "Dimensional Changes of $Nb_3Sn$ Rutherford Cables during Heat Treatment," *IEEE Trans. Appl. Supercond.*, submitted for publication

[7] E. F. Holik et al., "Fabrication and Analysis of 150 mm Aperture $Nb_3Sn$ MQXF Coils," *IEEE Trans. Appl. Supercond.*, submitted for publication

[8] H. Felice et al., "Design of HQ: a high field large bore $Nb_3Sn$ quadrupole magnet for LARP," *IEEE Trans. Appl. Supercond.*, vol. 19, no. 3, pp. 1235:11239, Jun. 2009.

[9] F. Borgnolutti et al., "Magnetic design optimization of a 150 mm aperture $Nb_3Sn$ low-beta quadrupole for the HiLumi LHC," *IEEE Trans. Appl. Supercond.*, vol. 24, no. 3, Jun. 2014, Art. ID. 4000405.

[10] E. Todesco, $4^{th}$ Joint HiLumi LHC-LARP Annual Meeting, Tsukuba. November 2014. http://indico.cern.ch/event/326148

[11] P. Ferracin, et al., "Magnet design of the 150 mm aperture low-$\beta$ quadrupoles for the high luminosity LHC," *IEEE Trans. Appl. Supercond.*, vol. 24, no. 3, pp. 1051:8223, Jun. 2013.

[12] S. Izquierdo et al., "Coil End Optimization of the Nb3Sn Quadrupole for the High Luminosity LHC," *IEEE Trans. Appl. Supercond*, vol. 25, no. 3, pp. 4001504, Jun. 2015.

[13] E. Todesco, J. Beauquis, B. Bellesia, G. Bevillard, G. Gubello, S. Pauletta, W. Scandale, C. Vollinger, E. Wildner, "Controlling field quality in magnet production," *LHC Performance workshop*, Chamonix XII, CERN-AB 2003-008 ADM (2003) 104-10

[14] R. Gupta, et al., "Tuning shims for high field quality in superconducting magnets," *IEEE Trans. On Magnetics*, Vol 32 No 4, 1996.

[15] G. Sabbi, et al., "Correction of high gradient quadrupole harmonics with magnetic shims," *IEEE Trans. Appl. Supercond.*, vol. 10, no. 1, 2000

[16] P. Hagen, "Study of magnetic shimming in triplet magnets," *HiLumi LHC Milestone Report 36*, 2013.

[17] P. Ferracin et al., Development of MQXF, the $Nb_3Sn$ low-$\beta$ Quadrupole for the HiLumi LHC," *IEEE Trans. Appl. Supercond.*, submitted for publication